An efficient approach to explore the solution space of a wind turbine rotor design process

Pietro Bortolotti,[1] Kristian Dixon,[2] Evan Gaertner,[1] Megan Rotondo,[2] and Garrett Barter[1]

[1] National Renewable Energy Laboratory, Boulder, Colorado
[2] Global Blade Innovation Center, Envision Energy, Boulder, Colorado

E-mail: pietro.bortolotti@nrel.gov
Keywords: MDAO, Rotor design, Blade design

Abstract. This study proposes a novel approach to explore the solution space of a wind turbine rotor design process. The goal is to offer to blade designers the possibility to select an optimal rotor for given market conditions, assessing trade-offs and alternatives in a matter of minutes. The design process consists of sequential aerodynamic-structural optimizations, where the two loops are linked via a blade-loading parameter that can be varied by the user. A design study is performed starting from the IEA Wind Task 37 land-based reference wind turbine. The solution space is characterized for rotor diameters in the range of 130–160 m, rated generator power values in the range of 3.0–6.0 MW, and tip-speed ratios in the range of 7.5–12.5. Results are discussed highlighting optimal design decisions and trade-offs.

1. Introduction

Growing competition among wind turbine manufacturers is putting pressure on turbine designers to devise tailored solutions for different markets while reducing development times for new products, which are pushed to market with increasing frequency. As the wind turbine rotor design process is a multiobjective, multiconstraint optimization problem, automated systems' engineering toolsets are increasingly adopted to assist designers in exploring the space of feasible solutions and selecting optimal blade designs. The literature offers a variety of approaches to the aerostructural design optimization of wind turbine rotors, where the key difference lies in the way loads are estimated. Studies have simulated the loading originating from steady-state storm wind [1, 2], steady-state rated wind [3, 4], steady-state condition mimicking a wind gust [5], and a simplified dynamic aeroservoelastic simulation mimicking loads from a full design load basis [6]. These frameworks suffer the risk of not representing the loads correctly and alternative approaches embed the actual design load cases into nested optimization algorithms [7]. The latter family of approaches runs however into significantly higher computational costs, with run times in the order of 10^2 hours for single-objective studies.

This work proposes a rotor aerostructural surrogate model that offers the possibility of exploring the solution space of a wind turbine rotor design problem in a matter of minutes while preserving the ability to evaluate constraints generated by both ultimate and fatigue loads. The design approach is here used to describe the solution space of land-based wind turbines in terms of performance, mass, and costs at varying design parameters.

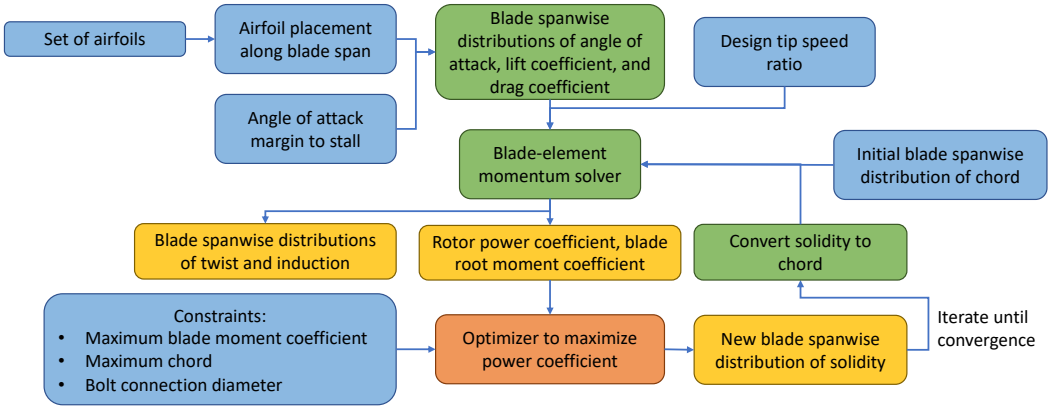

Figure 1. Scheme of the aerodynamic design loop. Color code: blue=user inputs, yellow=outputs, green=computations, orange=optimizer.

2. Design Approach

The wind turbine blade design process is inherently aerostructural, and an optimal design solution consists of a trade-off between the two disciplines. The next two subsections elaborate how the design problem is solved first in terms of the blade outer shape and then the inner structure, linking the two loops via the blade root flapwise moment coefficient, which is a nondimensional loading metric that describes the principal aerodynamic loading on the blade.

2.1. Aerodynamic Design

The first step of the process consists of designing the blade outer shape. The workflow, which is schematically represented in Fig. 1, optimizes the local solidity distribution along the blade span to maximize the rotor power coefficient. Local solidity is defined as:

$$\sigma = \frac{B \cdot c}{r} \tag{1}$$

where B is the number of blades, c the local chord distribution, and r the position along the blade span in the rotor coordinate system. The first inputs to the aerodynamic design loop, colored blue in Fig. 1, consist of a predefined set of airfoils, their placement along the blade span, and a margin between the design angles of attack and the stall angles along the blade span. With the angles of attack determined, the lift and drag coefficients along the span are determined from the airfoil polars. These quantities, in addition to the design tip-speed ratio, are fed to an inverted blade-element-momentum (BEM) model. The BEM model, which in this implementation is a modified version of the one presented by Ning 2014 [8], outputs the blade spanwise distributions of twist and axial induction, power coefficient, and blade root flapwise moment coefficient (C_m). C_m is a nondimensional representation of the aerodynamic loading, and it is here defined as:

$$C_m = \frac{B \cdot M_{f/r}}{\frac{1}{2} \cdot \rho \cdot A \cdot V_\infty^2 \cdot R} \tag{2}$$

where $M_{f/r}$ is the flapwise moment at the blade root, ρ is the air density, A is the rotor area here assumed excluding rotor cone and nacelle tilt angles, V_∞ is the undisturbed wind speed, and R is the rotor radius. Note that the aerodynamic design process analytically determines the optimal twist by inverting the BEM equations. This is different compared to traditional approaches that treat twist as an independent design variable and obtain the twist distribution

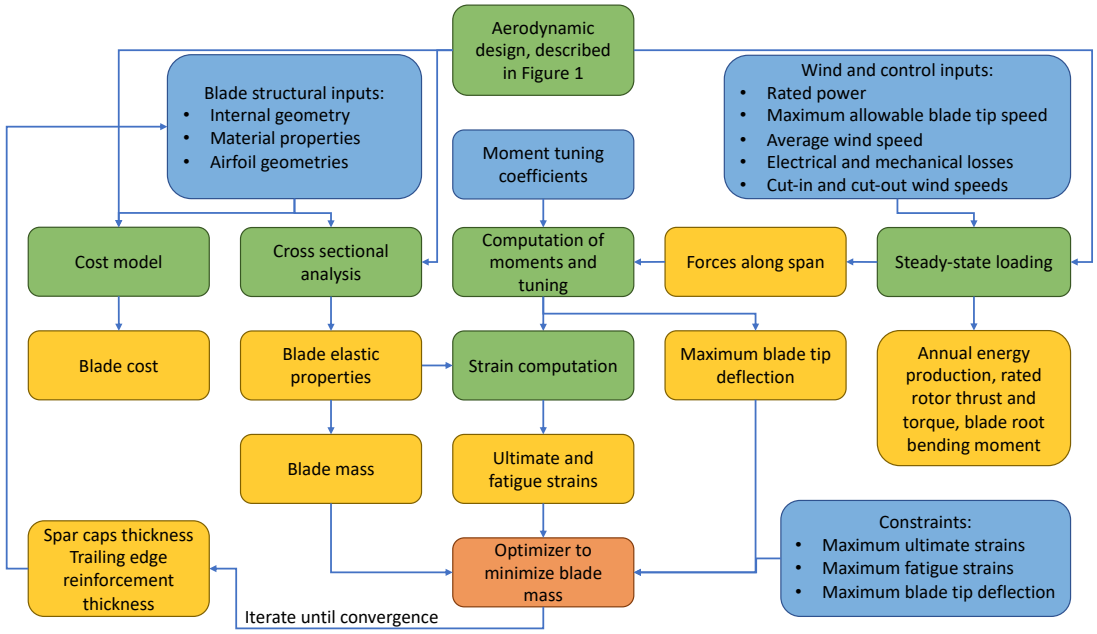

Figure 2. Scheme of the aerostructural design loop. Color code: see Fig. 1.

from the optimizer. This approach has the clear advantage of facilitating convergence, reducing the number of function calls and iterations, especially compared to traditional methods of inverse design. The limit of this approach is that it hides solutions where the blade twist is different than the aerodynamic optimum. One such case occurs when twist is decreased in the blade outer span, causing structural advantages that compensate for the loss in aerodynamic performance. Nonetheless, these design solutions could be investigated by introducing a margin to stall variable along the blade span, likely higher toward the blade tip, and running a parameter study around this distribution.

Power and moment coefficients are fed to a gradient-based optimizer that optimizes blade solidity along the span to maximize the power coefficient while constraining C_m to a maximum value $C_{m_{max}}$. The values of bolt connection diameter (which is the diameter of the circle drawn around the centers of the bolts at the blade root) and maximum chord are also constrained. The optimizer iterates until convergence is achieved within a desired tolerance for both figure of merit and constraints. When implemented efficiently, this optimization problem runs in a matter of seconds on a single core, and it is therefore well-suited to run design sweeps for a range of values of tip-speed ratio, $C_{m_{max}}$, and airfoil sets and their corresponding spanwise placement.

2.2. Aerostructural Design

Once the solidity-focused aerodynamic design is completed, the blade outer shape can be fed to a structural design optimization that minimizes blade mass under a set of constraints. A scheme of this design loop is shown in Fig. 2. In the current implementation, the design variables representing the blade structure are the thicknesses of the spar caps and trailing edge reinforcement along the blade span. Fairly simply, it would be possible to add design variables parameterizing more structural components of the blade, such as the skins and cores of the outer shell and of the shear webs. The constraints limit the maximum allowable blade tip deflection and material-specific ultimate strains along the span. The key element of this module is the load estimation, which is a surrogate model based on steady-state BEM simulations using multiplicative factors of the bending moments computed along the blade. These are determined

by first running a sweep of the design load cases prescribed by the International Electrotechnical Commission (IEC) standard 61400-1 [9] for a reference wind turbine design, and by later tuning the maximum bending moment and deflections obtained during steady-state simulations.

To size the spar caps, a BEM simulation is run at rated conditions, estimating the lift and drag forces along the blade span. The total forces are computed by adding centrifugal and gravity loading to the aerodynamic forces, and are then integrated twice along the blade span to obtain the flapwise bending moment distribution. This distribution is compared to the distributions corresponding to ultimate strains and maximum tip deflection spanwise loading distributions obtained during a sweep of design load cases (DLCs), and a polynomial tuning factor, k_p, is used to reconstruct the critical moments along the span from the steady-state distribution obtained at rated conditions:

$$k_p = a \cdot (1 - \eta)^2 + b \cdot (1 - \eta) + c \tag{3}$$

where η is the nondimensional span location and a, b, and c are tuning coefficients. The crucial aspect is that the coefficients are typically insensitive to a specific planform design, provided it is well-posed and evaluated within a limited range of rotor loading (W/m^2) and maximum tip speed. Such tuning coefficients may also be updated as part of an iterative design optimization process. By tuning k_p, constraints on strains in the spar caps can be defined to mimic constraints on ultimate and maximum blade tip deflection. Similarly, it is possible to tune the rated moments to a damage equivalent moment, which, once converted to strains, can be used to constrain the design problem.

For edgewise fatigue loading, the strains along the trailing edge are reconstructed by first extracting the gravity loading experienced by the blade at an azimuth angle of 90 degrees. The gravity forces are integrated twice along the span to compute the resulting bending moment M_g, which is then multiplied by tuning coefficients to reconstruct the moment distribution corresponding to the ultimate edgewise strains. To estimate fatigue strains, M_g is instead used to estimate a damage equivalent load:

$$M_{DEL} = \left((2 \cdot M_g)^m \cdot \frac{N}{N_{DEL}} \right)^{\frac{1}{m}} \tag{4}$$

where m is the Wohler's slope of the fatigue curve, N is the number of cycles experienced by the blade, and N_{DEL} is an equivalent number of cycles. N is estimated as:

$$N = N_y \cdot \int \Omega \cdot f_w \, dV \tag{5}$$

where N_y is the lifetime of the wind turbine in seconds, Ω is the rotor speed distribution along the wind speeds V of operation, and f_w is the Weibull probability density function of the wind speeds. The M_{DEL} along the blade span is multiplied by an elliptical tuning factor, k_e:

$$k_e = \frac{d}{\sqrt{1 - \eta}} \tag{6}$$

where d is the tuning coefficient in the equation. It should be noted that edgewise fatigue moments are dominated by gravity close to the blade root, whereas the outer span portions are affected by edgewise oscillations that originate from unsteady wind conditions and controller behavior. Edgewise oscillations suffer from poor aerodynamic damping, and it is important to account for them while sizing the trailing edge reinforcement. Compared to k_p, k_e is here adopted as it helps better match the moments in blade outer span compared to k_p.

In the current workflow, the elastic properties of the blade are computed from the two-dimensional cross-sectional analysis solver PreComp [5]. Given blade outer shape, internal geometry, and material mechanical properties, PreComp estimates the distributions of unit mass, edgewise stiffness, EI_{xx}, flapwise stiffness, EI_{yy}, axial stiffness, EA, and coordinates of the elastic center with respect to the pitch axis. To estimate blade tip deflection, these quantities are input together with the tuned moment distributions to the module pBEAM, a finite element code for beam-like structures using a 12-degrees-of-freedom Euler-Bernoulli beam element [5]. The strains, ϵ, are estimated at any location x and y of the blade structure in the reference system of the principal axes with the formula [5]:

$$\epsilon\left(x,y\right)=\frac{M_x}{EI_{xx}}\cdot y-\frac{M_y}{EI_{yy}}\cdot x+\frac{N}{EA} \tag{7}$$

Blade mass, tip deflection, and strains computed in the midpoint of the two spar caps and at the trailing edge are fed to a gradient-based optimizer, which iterates on the design variables until convergence is achieved. The workflow also includes a detailed blade cost model [10]. The model estimates the bill of materials, the number of labor hours and the cycle time, and the costs related to direct labor, overhead, buildings, tooling, equipment, maintenance, and capital for wind turbine blades in the range of 30–100 meters. The model applies to blades manufactured via vacuum-assisted resin transfer molding, which is the most commonly adopted manufacturing method for modern wind turbine blades. Blade cost can optionally be passed to the optimizer to run a blade cost minimization study.

As shown in Fig. 2, the aerodynamic and structural design loops are run sequentially for a sweep of input parameters—for example, rotor diameter and rated generator power. If a cluster or a workstation is available, each run can be executed in parallel, resulting in a computational time on the order of minutes. Given the very limited computational cost, it is straightforward to expand the dimensionality of the tradespace exploration by expanding the parameterization. This allows for additional design configurations to provide more insight on aerostructural trade-offs and coupling.

3. Results

The methodology is used to describe the solution space of rotors for land-based wind turbines. The inputs of the design model are taken from the 3.4 MW IEA Wind Task 37 reference wind turbine [11], which is briefly introduced in Sect. 3.1. The results of the aerodynamic design loop are presented in Sect. 3.2, whereas the results of the aerostructural optimization are presented in Sect. 3.3.

3.1. Initial Design

The IEA Wind Task 37 land-based reference wind turbine is class 3A, has a rotor diameter of 130 m, and a rated electrical power of 3.4 MW, totaling a rotor specific power of 250 W/m^2 [11]. The main inputs to the aerodynamic design loop are the spanwise distributions of lift and drag coefficients. These are here generated assuming a stall margin of 3 degrees and the airfoil positioning and the corresponding sets of polars of the reference wind turbine. The only change applied to the distributions is that two airfoils of the reference wind turbine, namely the flatback profile FX77-W-500 and the profile DU97-W-300, are removed from the list to generate a somewhat smoother and more realistic profile of the lift coefficient along the blade span. The distributions of lift and drag coefficients are shown in Fig. 3. The aerostructural design adopts as inputs the blade internal geometry of the reference wind turbine, namely a box-type load carrying structure with two spar caps with a constant width of 0.75 m and two shear webs running parallel along the span, trailing and leading edge reinforcements, and an outer shell made of skins and foam core. The composites are all glass

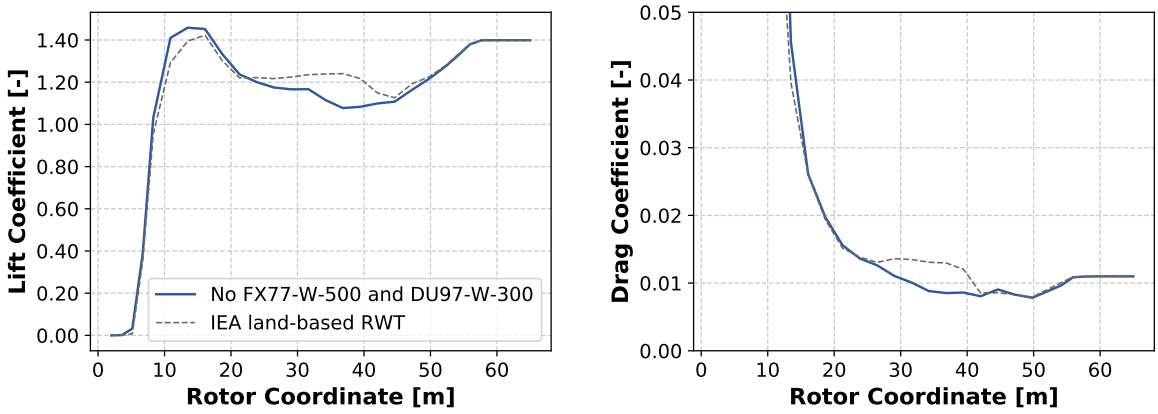

Figure 3. Distributions of lift and drag coefficients along the blade span assumed in this study and of the IEA land-based reference wind turbine

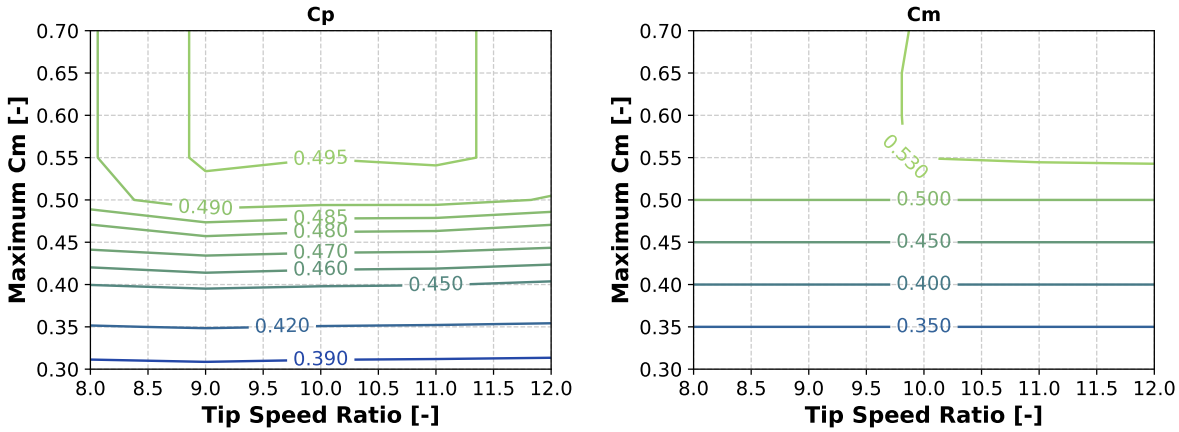

Figure 4. Contour plots of power and blade root flapwise moment coefficients showing the effect of the constraint of $C_{m_{max}}$

fiber fabrics and epoxy matrix, and the properties are specified in the open-source repository at: `https://github.com/IEAWindTask37/IEA-3.4-130-RWT`.

3.2. Aerodynamic Design Studies

A first aerodynamic design study is conducted, investigating the effect of $C_{m_{max}}$ on the aerodynamic design and performance. A sweep of five values of tip-speed ratio, equally spaced between 8 and 12, and nine values of $C_{m_{max}}$, equally spaced between 0.3 and 0.7, is run assuming the same rotor diameter of the reference wind turbine, namely 130 m. In the optimization, the bolt connection diameter is assumed to be 4.5% of the rotor radius, whereas the maximum allowable chord is assumed equal to 6% of the rotor radius. These two constraints are also adopted in the aerostructural optimization presented in Sect. 3.3.

The results in terms of power coefficient and moment coefficient are reported in Fig. 4. C_m is found not exceeding 0.53, above which the constraint on $C_{m_{max}}$ is no longer active and has no effect on the design solutions. The contour plots also show that the tip-speed ratio has no large effect on the aerodynamic performance of the rotor. This is partially because of the fact that Reynolds number effects are not considered here and, more importantly, for optimized planforms, $C_{p_{max}}$ is only weakly a function of tip-speed ratio for reasonable values corresponding

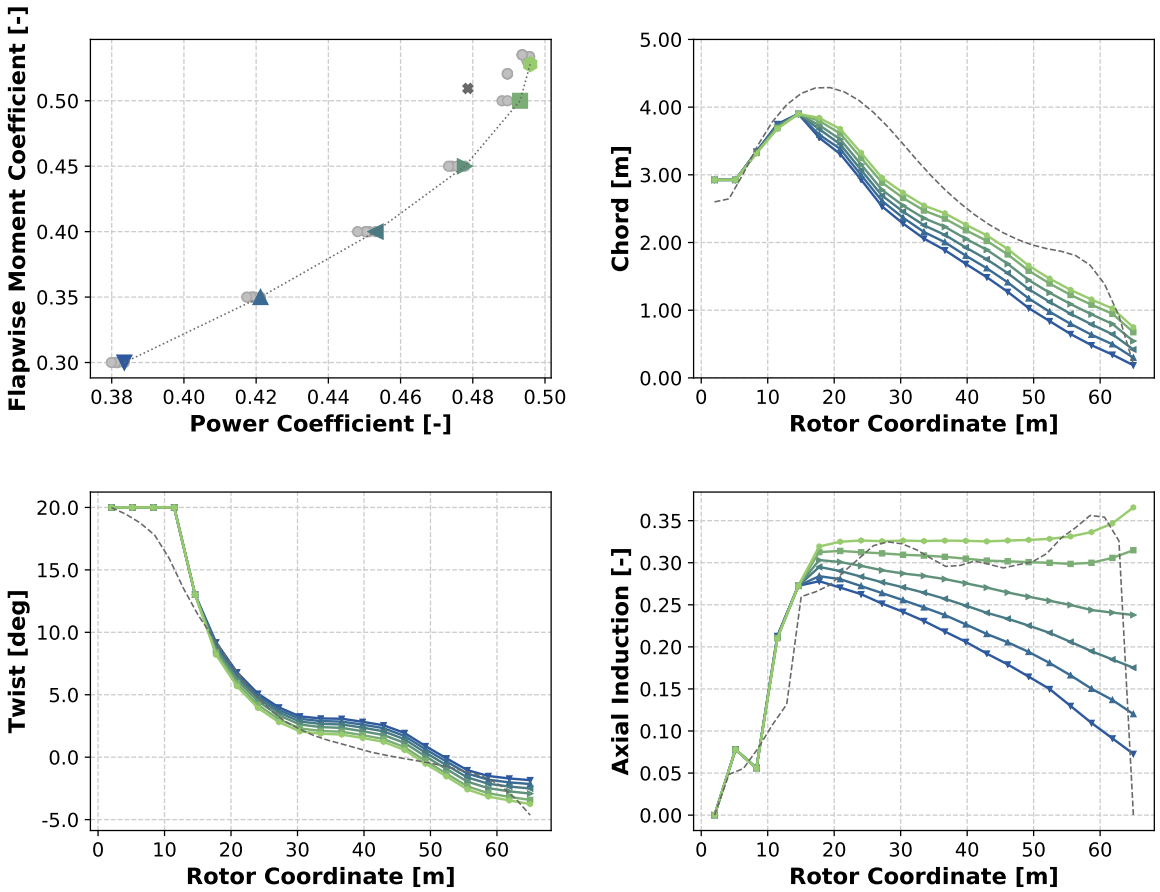

Figure 5. The plot in the top-left corner shows all design solutions at the varying maximum allowable moment coefficient $C_{m_{max}}$. The Pareto front is drawn with a dotted line. Along the front, six designs are highlighted with a different marker and color and their chord (top right), twist (bottom left), and axial induction (bottom right) are shown. The grey cross and the grey dashed lines correspond to the IEA reference wind turbine.

to contemporary horizontal-axis wind turbine blade design.

The same aerodynamic results can be visualized in terms of the relationship between power and moment coefficients, where a Pareto front is generated (see the top-left plot of Fig. 5). Along the front, six design solutions are extracted and their chord, twist, and axial induction distributions along the blade span are reported. The chord and axial distributions show that by decreasing the maximum allowable moment coefficient, the optimization solver increasingly unloads the outer portion of the blade by reducing the chord and obtaining lower values of axial induction and therefore lift. The twist distributions are instead the ones corresponding to the aerodynamic optimum, given the chord. It is worth stressing that twist represents an important degree of freedom to unload the rotor or otherwise change its aerodynamic state, and future research should investigate rotors with aerodynamically suboptimal twist distributions for a given design tip-speed ratio that instead optimize annual energy production for a given wind class or reduce blade/turbine loads.

As a comparison, the plots in Fig. 5 also report the chord, twist, and axial induction distributions of the IEA reference wind turbine with a grey dashed line, whereas the power and flapwise moment coefficients are plotted with a grey cross. Notably, the reference wind turbine has a much higher solidity than the blades designed here. This is a consequence of

	a	b	c	d
Ultimate flapwise	0.4378	0.0000	1.1954	–
Fatigue flapwise	0.1965	0.0000	0.6448	–
Ultimate tip deflection	0.0001	0.7237	0.5489	–
Ultimate edgewise	0.0000	3.0000	0.0000	–
Fatigue edgewise	–	–	–	0.9596

Table 1. Tuning coefficients for the aerostructural optimization

the 20% lower tip-speed ratio, set equal to 8.0 [11]. The power coefficient is also slightly lower than the values lying on the front, and the axial induction shows some oscillations around the optimum of one-third. This slightly suboptimal aerodynamic design may be the effect of modeling differences, or decisions taken by the optimizer of Cp-Max [7] during the aerostructural loops. These oscillations also provide a strong justification behind the method presented here. Handling the twist not as a direct design variable offers a higher degree of control over a crucial quantity, such as the aerodynamic twist. Overall, this helps gain trust in the results of the design process.

3.3. Aerostructural Design Studies

The aerostructural design process is used to explore the solution space at varying values of rotor diameter, between 130 and 160 m, and rated generator power, between 3.0 and 6.0 MW. The two ranges correspond to values of rotor-specific power between 150 and 450 W/m^2. The coefficients to tune the moments along the blade span are listed in Table 1. These are obtained by running operational (1.X) and storm (6.X) design load cases for an existing wind turbine using a basic time-domain controller. The design tip-speed ratio and the maximum allowable moment coefficient are assumed to be 10 and 0.49, respectively. For simplicity, the electrical and mechanical losses are assumed to be equal to 10% across all wind speeds. The optimization is constrained by the maximum allowable values of 4,000 $\mu\epsilon$ for ultimate strains, 2,000 $\mu\epsilon$ for fatigue strains, and tip deflection is limited to be smaller than 10% of the rotor radius.

The contour plots of annual energy production, rated rotor aerodynamic torque, blade mass, and blade cost are reported in Fig. 6. The results can be used by a rotor designer to select the right trade-off for given product requirements dictated by market conditions. Notably, some surfaces show trends that are smoother than others. The contour plot of blade mass shows that it is highly sensitive to diameter and only weakly dependent on rated power. This trend can be explained by the presence of region II1/2, where thrust and C_m decrease faster than the power coefficient. The result is that, at fixed tip-speed ratio, increasing the rated power simply enlarges region II1/2, mildly decreasing thrust loads at rated wind speed and ultimately generating small blade mass savings. An alternative design approach consists of not preassuming the tip-speed ratio, here fixed at 10, and set it to hit rated power and rated omega at the same wind speed. Such an approach would recover a strong dependence of blade mass to both diameter and power. It would also lead to slightly improved annual energy production and significantly heavier blades. The same contour plot of blade mass also shows that the design method presented here designs the blades of the reference wind turbine two tons lighter. It is also interesting to note that blade cost does increase with rotor diameter, but the increase in blade mass is not directly proportional to the increase in costs. Similar contour plots can be generated for other quantities, such as rated thrust, maximum tip deflection, or maximum ultimate and fatigue strains. The latter plots would show that for the given input conditions, all blades have the spar caps' thicknesses driven by tip deflection and ultimate strains, whereas fatigue drives the thickness of the trailing edge reinforcement. The constraint on fatigue strains in the spar caps is not active.

A second set of design sweep is generated at varying combinations of rotor diameter, ranging

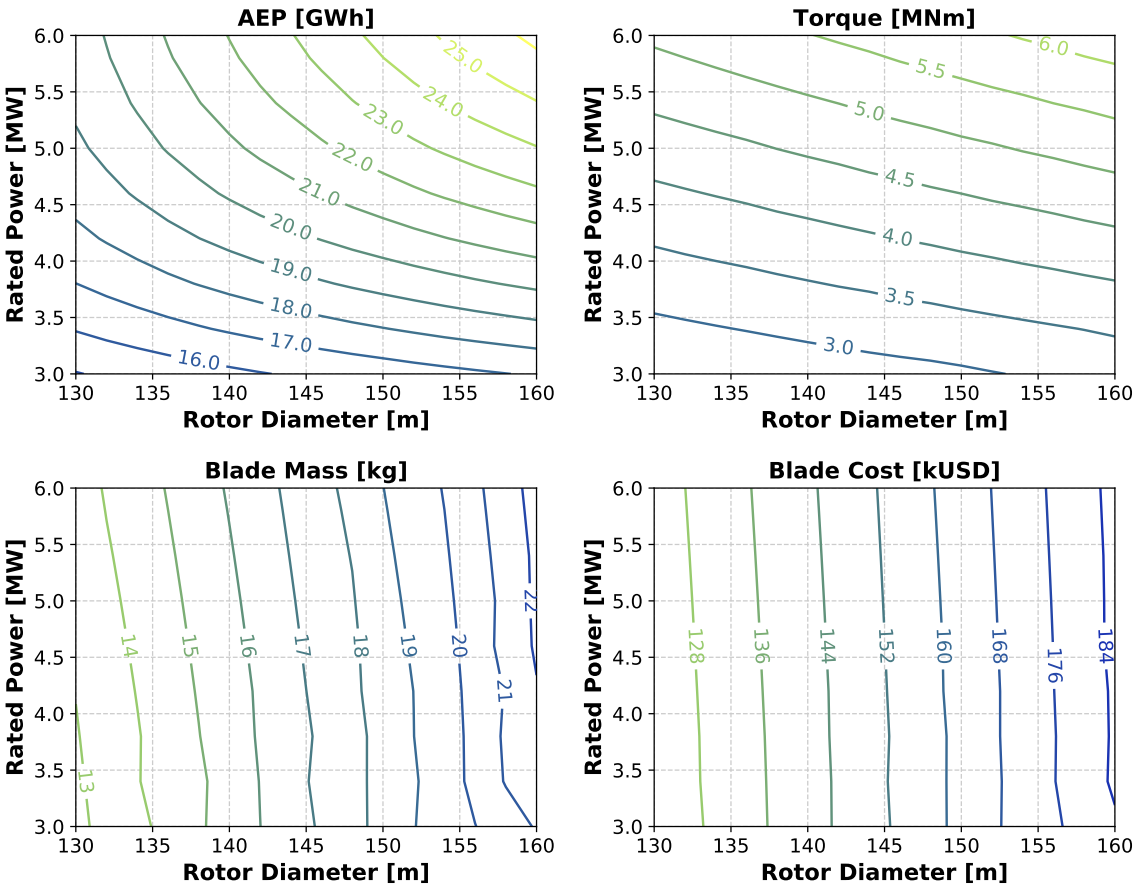

Figure 6. Contour plots of annual energy production, rated rotor torque, blade mass, and blade cost at varying rotor diameter and rated power values

between 130 and 160 m, and tip-speed ratio, ranging between 7.5 and 12.5, at a rated power of 3.4 MW. The results are shown in Fig. 7. The contour lines clearly highlight that a power output maximization leads to blade designs with a tip-speed ratio between 9 and 10. Below this value, the maximum allowable chord limits the aerodynamic efficiency, whereas above this value the constraint on maximum allowable blade tip speed causes power losses. Blade mass also exhibits a nonlinear trend, with a steep increase in blade mass at a higher tip-speed ratio because of the reduced rotor solidity, which leads to low area moments of inertia and thicker internal laminates. At tip-speed ratios above 12.5, the optimization solver struggles to find viable solutions. Interestingly, like annual energy production, blade cost shows an optimum at a tip-speed ratio equal to 10. Above this value, the high blade mass causes higher material costs, whereas lower tip-speed ratios cause an increase in blade mass because of the higher planform area that impacts tooling costs [10]. Finally, the plots help designers monitor the design drivers, and the contour of tip deflection shows how the tip deflection constraint is only active above rotor diameters of 140 m and tip speed ratios of 9. In this region, the tip deflection hits its maximum allowed, which is set at 10% of the rotor diameter, and the contour lines are vertical. Below this threshold of rotor diameter and tip-speed ratio, the blades are designed to respect the limits on ultimate and fatigue strains, and tip deflection is below its maximum allowable.

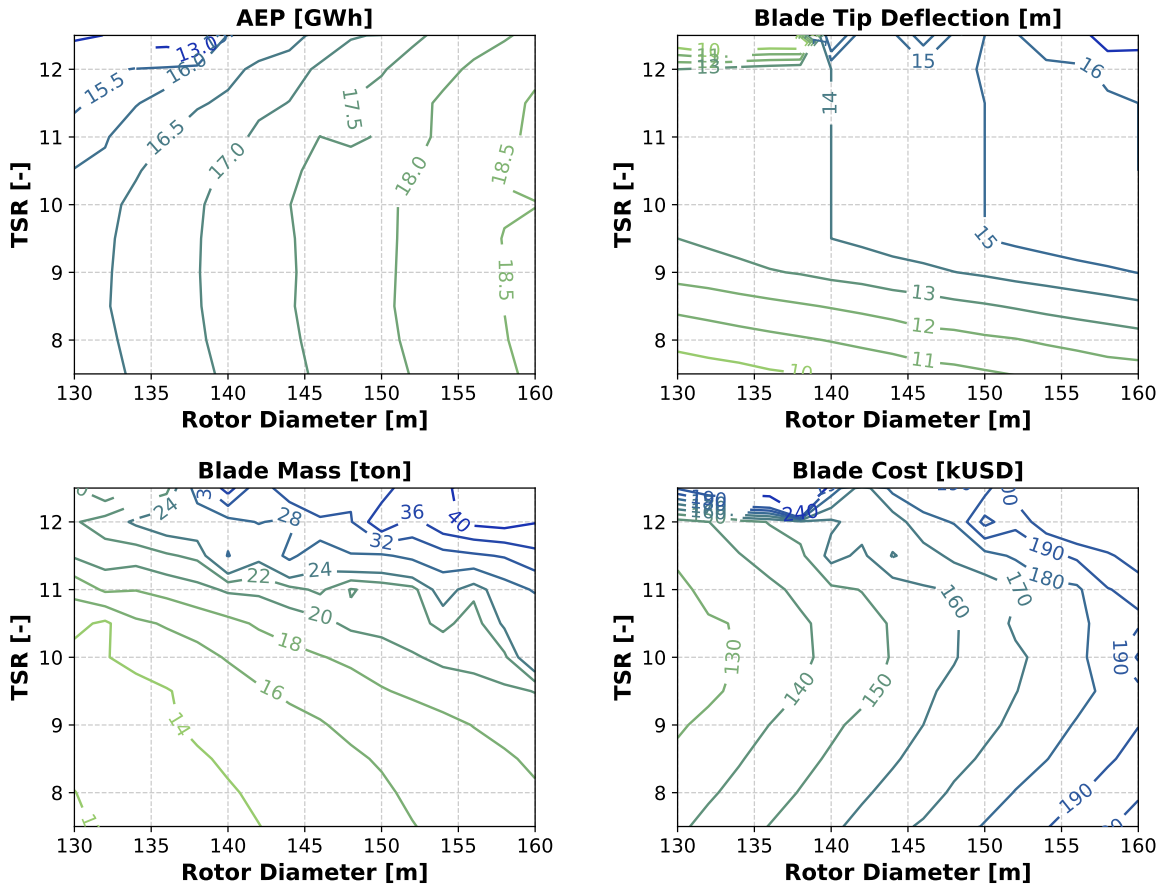

Figure 7. Contour plots of annual energy production (AEP), maximum tip deflection, blade mass, and blade cost at varying rotor diameter and tip-speed ratio values

4. Conclusions

This work proposes an efficient approach to investigate design solutions of a wind turbine rotor design. The framework, which runs in a matter of minutes, is first described and later exercised on a sweep of designs for rotor diameters between 130 and 160 m, rated power values between 3.0 and 6.0 MW, and tip-speed ratios between 7.5 and 12.5. The results are presented in terms of Pareto fronts and design space contour plots, providing a useful tool for wind turbine designers to assess different trade-offs and optimal solutions. The framework will be expanded to support a richer parametrization of the blade structure and the setup of links to the design modules of the rest of the turbine system, such as the drivetrain, generator, and tower.

Acknowledgments

The authors would like to acknowledge Katherine Dykes for initiating the project. A portion of the research was performed using computational resources sponsored by the U.S. Department of Energy's Office of Energy Efficiency and Renewable Energy and located at the National Renewable Energy Laboratory. This work was authored in part by the National Renewable Energy Laboratory, operated by Alliance for Sustainable Energy, LLC, for the U.S. Department of Energy (DOE) under Contract No. DE-AC36-08GO28308. Funding provided by the U.S. Department of Energy Office of Energy Efficiency and Renewable Energy Wind Energy Technologies Office. The views expressed in the article do not necessarily represent the views of

References

[1] Fuglsang, P. and Madsen, H.A. *J. Wind. Eng. Ind. Ae.*, 1999;80:191-206. doi: 10.1016/S0167-6105(98)00191-3
[2] Bottasso, C.L., et al. *J. of Physics, Conference Series*, 2014;524. doi: 10.1088/1742-6596/524/1/012041
[3] Benini, E., and Toffolo, A. *ASME J. of Solar Energy Engineering*, 2002;124(4):357-363. doi: 10.1115/1.1510868
[4] Fischer, G.R., et al. *Renewable Energy*, 2014(62):506-515. doi: 10.1016/j.renene.2013.08.009
[5] Ning, A. and Petch, D. *Wind Energy*, 2016;19(12): 2137-2152. doi: 10.1002/we.1972.
[6] Pavese, C., et al. *J. of Physics, Conference Series*, 2016;753. doi: 10.1088/1742-6596/753/6/062005
[7] Bortolotti, P. et al. *Wind Energ. Sci.*, 2016;1(1): 71-88. doi: 10.5194/wes-1-71-2016.
[8] Ning, A. *Wind Energy*, 2014;17(9): 1327-1345. doi: 10.1002/we.1636.
[9] Internal Electrotechnical Commission IEC, 61400-1. Wind turbines – Part 1: Design requirements. 2005.
[10] Bortolotti, P. et al. NREL/TP-5000-73585, 2019. `https://www.nrel.gov/docs/fy19osti/73585.pdf`.
[11] Bortolotti, P. et al. NREL/TP-5000-73492, 2019. `https://www.nrel.gov/docs/fy19osti/73492.pdf`